How cellulose nanofibrils and cellulose microparticles impact paper strength - A visualization approach

Carbohydrate Polymers 254 (2021) 117406

Contents lists available at ScienceDirect

Carbohydrate Polymers

journal homepage: www.elsevier.com/locate/carbpol

How cellulose nanofibrils and cellulose microparticles impact paper strength—A visualization approach

Mathias A. Hobisch [a], Simon Zabler [b], Sylvia M. Bardet [c], Armin Zankel [d], Tiina Nypelö [e,f], Rene Eckhart [a], Wolfgang Bauer [a], Stefan Spirk [a,*]

[a] Institute of Bioproducts and Paper Technology, Graz University of Technology, A-8010 Graz, Austria
[b] Fraunhofer IIS, Josef-Martin-Weg 63, 97074 Würzburg, Germany
[c] CNRS, XLIM, UMR 7252, Université Limoges, F-87000 Limoges, France
[d] Institute of Electron Microscopy and Nanoanalysis, NAWI Graz, Graz University of Technology and Centre for Electron Microscopy, Steyrergasse 17, 8010 Graz, Austria
[e] Wallenberg Wood Science Center, Chalmers University of Technology, 412 96 Gothenburg, Sweden
[f] Department of Chemistry and Chemical Engineering, Chalmers University of Technology, 412 96 Gothenburg, Sweden

ARTICLE INFO

Keywords:
Cellulose nanofibrils
Cellulose
Paper
Cellulosic fines
X-ray microtomography
Confocal laser scanning microscopy
Multiphoton microscopy

ABSTRACT

Cellulosic nanomaterials are in the focus of academia and industry to realize light-weight biobased materials with remarkable strength. While the effect is well known, the distribution of these nanomaterials are less explored, particularly for paper sheets. Here, we explore the 3D distribution of micro and nanosized cellulosic particles in paper sheets and correlate their extent of fibrillation to the distribution inside the sheets and subsequently to paper properties. To overcome challenges with contrast between the particles and the matrix, we attached probes on the cellulose nano/microparticles, either by covalent attachment of fluorescent dyes or by physical deposition of cobalt ferrite nanoparticles. The increased contrast enabled visualization of the micro and nanosized particles inside the paper matrix using multiphoton microscopy, X-ray microtomography and SEM-EDX. The results indicate that fibrillary fines enrich at pores and fiber-fiber junctions, thereby increasing the relative bonded area between fibers to enhance paper strength while CNF seems to additionally form an inner 3D network.

Hypotheses

The spatial distribution of micro and nanosized cellulosic particles in paper is challenged by several methods.

1. Introduction

The market for paper has been steadily growing over the past decades but traditional products such as newsprint showed a tremendous decline which is expected to continue. To compensate for this gap, new products in the field of packaging are currently developed to improve paper properties with a focus on mechanical properties. In the development pipelines of pulp and paper companies, different forms of fibrillar cellulosic particles are currently explored for such purposes. Particularly cellulose microfibrils and cellulose nanofibrils (CMF/CNF) are considered as strength additives in paper manufacturing. The main difference between these materials is their degree of fibrillation resulting in different diameters and shapes. CNF for instance is a highly fibrillated material with diameters of a few nanometers while in CMF the elementary fibrils are not fully separated yielding diameters in the microscale (Nechyporchuk, Belgacem, & Bras, 2016; Yousefi, Azad, Mashkour, & Khazaeian, 2018). Cellulosic fines, already present in the pulp, in turn contain also larger fragments and their definition is rather arbitrary. TAPPI defines cellulosic fines as small enough to pass a 200 mesh screen (TAPPI, 1994), which is equivalent to 76 μm whole diameter and with a microscopic length of maximum 200 μm (Hyll, Farahani, & Mattsson, 2016). In literature, fines are further segmented in primary and secondary fines. Primary fines can be isolated after chemical pulping and tend to have a flake like structure, whereas secondary fines predominate after the refining process increasing the degree of fibrillation (Krogerus, Fagerholm, & Tiikkaja, 2002).

The addition of highly fibrillar particles during paper manufacturing

* Corresponding author at: Institute of Bioproducts and Paper Technology, Graz University of Technology, Graz, Austria.
E-mail address: stefan.spirk@tugraz.at (S. Spirk).

https://doi.org/10.1016/j.carbpol.2020.117406
Received 22 June 2020; Received in revised form 7 November 2020; Accepted 12 November 2020
Available online 23 November 2020

impacts furnish and paper technological properties in several ways. Important properties of the furnish are typically water retention value, and of the paper sheet density, air permeability and the tensile index, which all are strongly affected by the presence of fibrillated celluloses (Odabas, Henniges, Potthast, & Rosenau, 2016). Fine cellulosic materials feature a higher water binding capacity causing problems in dewatering and sheet forming, since both parameters are strongly affected by the degree of fibrillation of the added particles (Afra, Yousefi, Hadilam, & Nishino, 2013; Kang & Paulapuro, 2006). Sirviö and Nurminen for instance investigated the influence of fines content on porosity/density, tensile index and light scattering behavior of paper sheets (Sirviö & Nurminen, 2004). They observed an increase in density of the paper sheets concomitant with an increase in tensile index, proportional to the amount of fibrillar fines in the sheets. The addition of fibrillar fines to the sheets did not alter the light scattering properties of the sheets (in contrast to flake like particles, which influenced light scattering). These results pointed at an enrichment of fine fibrillar material in the pores as well as in fiber-fiber bonds. However, they did not support their hypothesis by localization of the fines inside the sheets. In dry state, the presence of CNF leads to higher densities of paper sheets, resulting in lower air permeability and higher mechanical strength. Although there is a correlation with the degree of fibrillation, effects are not linear. It has been suggested that the formation of an inner 3D network of highly fibrillated particles within the paper sheet stabilizes the fiber network, thereby improving strength and increasing density (Bossu et al., 2019; Nanko & Ohsawa, 1989). Most publications so far investigate the interactions between fibers and CNF, CMF or pulp fines, without considering morphological differences of the additives and their 3-dimensional distribution inside the fibrous network. One of the very few studies focusing on the localization (though not in a 3D approach) of fine materials inside paper sheets was reported by Nanko and Ohsawa who studied the role of fines in sheet forming using transmission electron microscopy, SEM and confocal laser microscopy (Nanko & Ohsawa, 1989). They showed that upon fibrillation during pulp refining, the resulting fines – external fibrils and secondary fines - aggregate in fiber-fiber bonds, as well as in pore walls upon sheet forming. For imaging of the fines, they used labelling techniques incorporating gold and palladium nanoparticles to achieve contrast in transmission electron microscopy. In addition, there are several accounts on CNF labelling using different approaches to study CNF migration or leaching from paper-based products (Ding et al., 2018; Huang et al., 2020; Purington, Bousfield, & Gramlich, 2019; Reid, Karlsson, & Abitbol, 2020; Salari et al., 2019).

In the past years, we have been building on this seminal work of Nanko and Ohsawa and developed different strategies to visualize cellulosic fines in paper sheets using two independent labeling techniques based on fluorescence and chemical contrast (Hobisch, Muller et al., 2019; Hobisch, Bossu et al., 2019). Detection was accomplished by fluorescence microscopy, multiphoton imaging, X-ray microtomography and scanning electron microscopy with energy dispersive X-ray spectroscopy. The combination of these methods allowed for a localization of the fines in paper sheets and resulted that the fines accumulate in pore walls as well as on fiber-fiber bonds.

In this paper, we apply the previously developed methods to other small-scale cellulosic particles. The hypothesis of this study is whether and to which extent their fibrillation impacts paper properties and how this correlates to their distribution inside paper sheets. We visualize the interactions within the sheet with X-ray and light microscopic based imaging techniques. The labeling methods are not limited to applications with paper and board, revealing opportunities to provide further insights into the interactions between micro- and nanofibrillar lignocelluloses in various polymeric composites. The design of the study involves the production/separation of micro- and nanostructured particles with a specific morphology (i), labeling them with two different approaches (ii), preparation of handsheets with labeled and non-labeled particles (iii) determination of mechanical and physical parameter of pulps and handsheets (iv) and imaging analysis of the handsheets (v). We aim to provide data by combination of the methods and the comparison of different fibrillation degrees in a single study. Further, we use whitewater circulation which yields a nearly quantitative retention of the cellulosic particles in the handsheets regardless of the size, which is hardly provided in other studies.

2. Experimental part

2.1. Materials

$CoCl_2 * 6\ H_2O$ (98.0 %) and $FeSO_4 * 7\ H_2O$ (99.0 %) were supplied by Fluka (Buchs, Switzerland), KNO_3 (99.6 %) and NaOH (99 %) were obtained from VWR chemicals (Radnor, USA). Epichlorohydrin (>99 %) and ammonium chloride/ammonium hydroxide buffer solutions (NH_4Cl, 1 wt.%; NH_4OH, 4 wt.% (pH 10–11) were purchased from Sigma-Aldrich (Vienna, Austria). Rhodamine B isothiocyanate (mixed isomers) was supplied by Cayman Chemical (Ann Arbor, USA). All chemicals were used without further purification.

An industrially refined bleached, sulfite pulp (mixture of spruce and beech; 18 °SR, according to ISO 5267-1, lignin content below 1 wt.%) was the source of fines and further used for the paper sheet preparation. The CNF was obtained from University of Maine, USA (produced via mechanical refining). According to the manufacturer, bleached softwood kraft pulp was mechanically treated in order to produce cellulose nanofibrils (average width 50 nm, length several microns). Fiber fragments (AF) were supplied from ARBOCEL® (BE 600/30 PU) with average geometry of 40 µm x 20 µm, showing hardly any fibrillation. Pulp fines (SF) were separated from industrially refined sulfite pulp using a pressure screen, following a published routine (Fischer et al., 2017). The pulp was diluted with water to a consistency to 1 wt.%, and allowed to stir for about 10 min. Afterwards, the suspension was pumped through the pressure screen, whose main element is a perforated screen with a hole diameter of 100 µm. Large particles incapable of passing the pressure screen were transferred back to the feed chest, while the fines fraction was collected in a separate chest. The procedure was repeated until the fines content of the pulp was lower than 1 wt.% according to SCAN-CM 66:05 (Dynamic Drainage Jar). The resulting fines suspension was pumped to a dissolved air flotation cell, to increase fines' consistency from 0.02 to 0.5 wt.%. Details on the design of the flotation cell can be found elsewhere (Fischer et al., 2017). All concentrations were determined in triplicate by a gravimetric approach. The resulting fines features a CED^2 value of 34.1 µm determined by the L&W fiber tester. Carbohydrate composition (Table 1a) was analyzed via sulfuric acid hydrolysis according to (Theander & Westerlund, 1986) using high performance anion exchange chromatography with pulsed amperometric detection (HPAEC-PAD) and Dionex ICS 3000 ion chromatography system equipped with a CarboPacPA1 analytical column. Fucose was used as internal standard. The acid soluble lignin was determined measuring absorbance at 205 nm using the same dilute hydrolysate as used for the carbohydrate composition determination. The concentration of the acid soluble lignin was calculated using the Lambert-Beer law and was 1.0 (AF), 1.1 (SF) and 0.9 wt.% (CNF).

Table 1a
Carbohydrate composition of the different cellulose materials. All values are given in wt.%.

	AF	SF	CNF
Ara	0.0	0.0	0.9
Rha	0.0	0.0	0.0
Gal	0.0	0.0	0.0
Glu	81.4	90.2	83.0
Xyl	17.1	5.6	8.9
Man	1.5	4.2	7.2
Total	100.0	100.0	100.0

2.2. Nanoparticle labeling

A specific amount (10 % of the whole sheet) of cellulosic substituents was weighed and suspended in water (1 wt.%). The suspension was ultrasonicated and exhaustively stirred to disperse cellulosic particles. Afterwards, salts were added (3.3 g, 0.033 mol $CoCl_2$ * 6 H_2O; 7.7 g, 0.066 mol $FeSO_4$ * 7 H_2O) and the suspension was stirred for a period of 3 h at 90 °C. The impregnated celluloses were separated from the solution by centrifugation. The impregnated celluloses were added to a solution containing 1.27 g KNO_3 (12 mmol) and 5.5 g NaOH (139 mmol) in 420 mL distilled water at 90 °C. The color of the suspension changed immediately from white to brownish, indicating growth of NPs. After 1 h, the colored particles were extensively washed until a pH value of 7 was reached and then again centrifuged. NP content on the cellulosic particles was determined by thermogravimetric analysis. For this purpose, a labeled and an unlabeled sample was measured for each type of NP. The ash content of the unlabeled sample was subtracted from the labeled ones to determine the inorganic content. NP content of 30 (CNF), 24 (secondary fines), and 4 wt.% (ARBOCEL® fibers) have been determined.

2.3. Fluorescence labeling

Cellulosic substituents were dyed following the routine of Hobisch et al. (Hobisch, Bossu et al., 2019). First, celluloses (3.6 g) were diluted to a 1 wt.% suspension, exhibiting a dried mass equal to 10 % of the dried mass of the pulp. Second, 5 mL· epichlorohydrin (64 mmol) per gram cellulose was added to the suspension, changing the pH to 12. The suspension was stirred over 2 h at 60 °C, followed by an extensive washing step with distilled water until neutral. Third, the suspension was redispersed to an 1 wt.% suspension, adding 5 mL ammonium chloride ammonium hydroxide buffer (3.4 mmol NH_4Cl; 21 mmol NH_4OH) per gram of cellulose. The alkaline solution (pH 10–11) was steadily stirred for 2 h at 60 °C, introducing the amino group. Again, excessive reagent was removed by extensive washing with distilled water. Fourth, 0.01 g RBITC (Rhodamine B isothiocyanate, 19 μmol) was added for each gram of cellulose, and the solution was stirred for a period of 24 h at room temperature under exclusion of light. Afterwards, the suspension was extensively washed to remove excess of non-reacted dye.

2.4. Handsheet preparation and analysis

The sulfite pulp after the separation of fines (residual fines content 1%) was used for handsheet forming. After disintegration (ISO 5263-1) of the cellulose blends, handsheets were formed on a Rapid-Köthen sheet former (FRANK-PTI) with a grammage of 60 g m^{-2}, applying white water recirculation (Giner Tovar, Fischer, Eckhart, & Bauer, 2015). Ten different sheet types were prepared: a blank,- and in each case three types of sheets containing 10 % untreated, nanoparticle labeled and stained cellulosic particles (CNF, secondary fines and ARBOCEL® fiber fragments respectively, see Table 1b). After discarding the first five handsheets, eight handsheets were formed and dried (ISO 5269-2:2004) per blend to later determine apparent density (ISO 534:2011), tensile index (ISO 1924-2:2008, FRANK-PTI tensile tester) and air permeability according to Bendtsen (ISO 5636-3:2013). The water retention value of the furnishes was evaluated according to the ISO 23714:2014, comparing the impact of the cellulosic substituents and the labeling process on the swelling behavior of the pulp.

2.5. Low voltage – scanning electron microscopy (SEM)

The surface of the labeled particles was visualized by Low Voltage – Scanning Electron Microscopy (LV-SEM) on the C-band using the Everhart-Thornley type of detector of the high-resolution scanning electron microscope Zeiss Sigma VP 300 (Zeiss, Oberkochen, Germany).

Table 1b
Overview and composition of the paper sheets for this study. NP labeled refers to Fe_2CoO_4 labeling, stained refers to fluorescent labeling. The blank (ECO) is not shown and consists of 100 % pulp.

	Cellulose nanofibrils		
Particles [%]	10	10	10
Pulp [%]	90	90	90
Treatment	Untreated	NP labeled	Stained
Abbreviation	CNF	nCNF	fCNF
	Secondary fines		
Particles [%]	10	10	10
Pulp [%]	90	90	90
Treatment	Untreated	NP labeled	Stained
Abbreviation	SF	nSF	fSF
	ARBOCEL® fiber fragment		
Particles [%]	10	10	10
Pulp [%]	90	90	90
Treatment	Untreated	NP labeled	Stained
Abbreviation	AF	nAF	fAF

In LV-SEM typically electron beam energies between 0.5 and 5.0 keV are used which allows the investigation of specimens without coating. However, for imaging cellulose specimens a beam energy of 0.65 keV has been verified to deliver most promising results (Fischer et al., 2014).

2.6. Cross section analysis via SEM

Paper sheets containing 10 % CNF, secondary fines and ARBOCEL® fibers and the blank, labeled as ECO were embedded in the resin "Epofix" (Struers GmbH, Willich, Germany) at room temperature. After hardening, the specimens were cut with an ultramicrotome (Leica EM UC6, Leica Microsystems Vienna, Austria) using a histo- diamond-knife (Diatome Ltd., Biel, Switzerland). A 10 nm thick layer of carbon was coated onto the freshly produced cross sections. For the microanalytic investigations the electron microscope ZEISS Sigma VP 300 (Oberkochen, Germany), equipped with a Schottky field emitter, was used for imaging the cross sections in the high vacuum mode (acceleration voltage of the primary electrons 3 kV). Secondary electrons (SE) were used for delivering a good topographic contrast showing the morphology of the different samples. Additionally, elemental analysis was performed using an SDD-detector (OXFORD, England) for energy dispersive X-ray spectroscopy (EDX). To obtain the distribution of different chemical elements, EDX mapping was performed at an acceleration voltage of 3 kV.

2.7. X-ray microtomography

Similar to our previous study we employ phase contrast submicrometer X-ray computed tomography (subμ CT) for recording three-dimensional volume images of different sheets of paper (loaded and unloaded, marked and unmarked). The Fraunhofer tabletop scanner "Click-CT" is designed for imaging organic and inorganic materials at the highest resolution. We employ 0.62 μm $voxel^{-1}$ object sampling for the images shown here, covering a field of view of 1.25 mm in diameter. Since the typical thickness of one sheet of paper is <0.2 mm we could record all papers stacked in one scan (total scan time 6.7 h). Volume image reconstruction, Paganin-type phase retrieval and Wiener deconvolution were routinely applied with the software PyXIT (Zabler et al., 2019). Maximum intensity projections along the longitudinal direction of the paper as well as histograms of the latter were computed with the software ImageJ2 (Hobisch, Muller et al., 2019).

Note that subμ-CT features material contrast which is dominated by electron density, hence atomic number and mass density (similar to backscatter electron images). Even features which are not spatially resolved by the scanner (typical resolution limit 0.9 μm) can be detected due to a shift of the average gray value, if a certain concentration of high-Z material is present in a pixel (e.g. in the form of ferritic NPs).

2.8. Confocal laser scanning microscopy

The cross sections of the sheets embedded in the resin "Epofix" were also analyzed by confocal laser scanning microscopy (FISH/CLSM) using a Leica TCS SPE confocal laser scanning microscope (Leica Microsystems, Mannheim, Germany) with oil immersion objective lenses Leica ACS APO 10.0 x CS, exciting cellulose at 405 nm and RBITC at 532 nm. The emission spectra between 420 and 500 nm visualizes the autofluorescence of lignin superimposed by the emission spectra of the fluorescence labeled samples which was determined between 550–600 nm.

2.9. Multiphoton microscopy

Two-photon excitation microscopy has also been used for the analysis of the fluorescence labeled particles. Paper sheets were positioned on a stage of a customized Olympus multiphoton microscope BX61WI/FV1200MPE with a 25X immersion objective (1.05NA, 2.0 mm working distance) coupled with a tunable femtosecond Ti:Sapphire pulsed laser (Chameleon Ultra II, Coherent) for the excitation (Bardet et al., 2016). Image stacks were acquired under 810 nm excitation for second harmonic generation (cellulose) and fluorescence (RBITC for smaller celluloses, autofluorescence for lignin) wavelength with FluoView FV1200 software (v4.1.1.5, Olympus). Each acquisition in photon-counting mode produces a 3D stack of 640 × 640 × 53 pi, with a sampling step of 2 µm and a dwell time of 20 µs·pi^{-1} (input laser 20 mW). The different components of the emitted light from the sample were separated using a dichroic mirror (450 nm) and detected by a pair of photomultiplier tubes preceded by fluorophore specific emission filters (607/36 for fluorescence in red, 405/10 for second harmonic generation in green). The obtained images were analyzed with Imaris software (Bitplane AG) or Fiji/ImageJ (NIH).

3. Results and discussion

3.1. Labeling approaches

Nanoparticles were attached to the cellulosic particles using an *in-situ* method (Olsson et al., 2010). The method employs cobalt and iron salts under alkaline conditions and generates Fe_2CoO_4 NPs (FCONPs) on the surface (Fig. 1a–c). The FCONPs were irreversible attached to the fibril surfaces as any leaching from the fibers in aqueous media was not observed. The amount of FCONPs on the surface of the cellulosic particles varies between the samples since their mophology is rather different. While CNF and secondary fines have rather high NP contents (30 and 24 w.t%, respectively), we were not able to produce ARBOCEL® fibers with NP contents higher than 4 wt.% as proven by thermogravimetric analyses.

Rhodamin B isothiocyanate was used for labeling resulting in a covalent attachment of the fluorophore on the cellulosic particles. Fig. 1d-f shows the fluorescence images (excitation: 532 nm, emission: 595 nm) of the different labeled cellulosic samples obtained on a confocal laser scanning microscope. A homogeneous distribution of the fluorophore was observed for all samples. The individual nanofibrils could not be visualized by CLSM due to limited resolution, but aggregates formed by storage in a fridge at 6 °C over a period of one month clearly showed fluorescence.

3.2. Sheet forming using non-labeled and labeled samples and effect on water retention, air permeability and tensile index

The next step in the visualization process was to produce sheets with labeled and unlabeled compounds and to evaluate the relevant paper technological parameters compared to the blank. As expected, the nature of additive (CNF, SF, AF, all added at 10 % w/w) alters the sheet properties even without labeling (Figs. S1 and S2a). For instance, the addition of CNF drastically increased water retention value (from 1.10 ± 0.01 for ECO to 1.32 ± 0.01 for CNF) and tensile index of the sheets

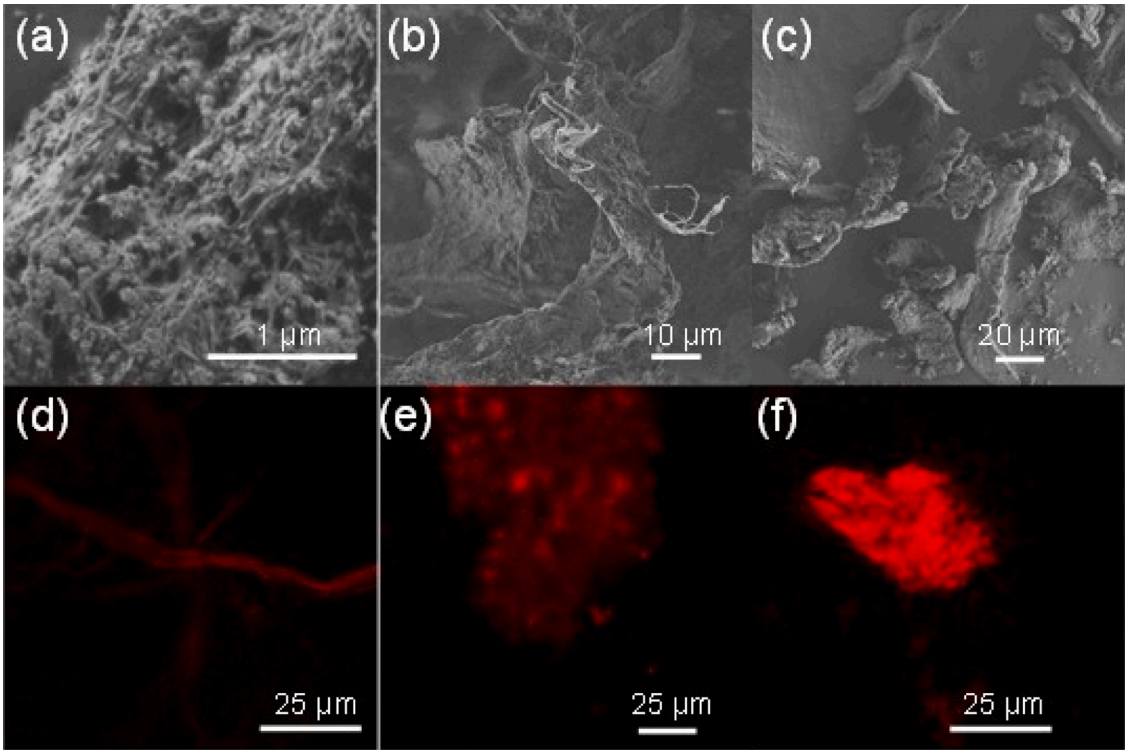

Fig. 1. Visualisation of labeled cellulose nanofibrils (a,d), secondary fines (b, e) and ARBOCEL® fibers (c, f) via scanning electron microscopy (nanoparticle labeling; a-c) and confocal laser scanning microscopy (fluorescence staining; d-f).

compared to the blank (36.2 ± 1.7 Nm g^{-1} for ECO vs 56.4 ± 3.8 Nm g^{-1} for nCNF). This increase is not as pronounced for secondary fines (46.7 ± 1.8 Nm g^{-1}) and absent for ARBOCEL® (32.7 ± 1.5 Nm g^{-1}) fibers (Figs. 2d-f and S3d–f). Air permeability (Fig. 2g-i) in turn was very low for the samples containing the CNF (165 ± 9 mL min^{-1}), while the SF are slightly higher (899 ± 72 mL min^{-1}). The sheets containing the AF in turn exhibited the same air permeability as the blank sample reaching the maxima of 5000 mL min^{-1}.

Differences between sheets containing labelled materials and non-labelled materials are minor and indicate that the sheet structure including porosity and density is only affected to a low degree by the labelling procedure. For example, the WRV, air permeability, density and tensile indexes of the sheets are in a similar range. However, as hydrogen bonding is slightly affected by the labeled materials, there are small effects on the individual parameters which are summarized in box plots depicted in the Supporting Information (Fig. S3). The only noteworthy deviation was observed in tensile index (56.4 ± 3.8 vs 50.5 ± 2.5 Nm g^{-1} for CNF and nCNF; 46.7 ± 1.8 vs 42.4 ± 1.8 Nm g^{-1} for SF and nSF; 32.7 ± 1.5 vs 31.3 ± 1.3 Nm g^{-1} for AF and nAF). When looking at the box plots of the tensile indexes (Fig. S3d–f), the values, however, are in a similar range considering the standard deviations.

These data suggest that the degree of fibrillation of the fine fibrous particles governs the sheet properties, which must relate to the localization inside the paper sheets and their interaction with macroscopic pulp fibers. Therefore, the sheets were subjected to different visualization techniques. Fluorescence stained particles (fCNF, fSF, fAF) can be excited enabling the application of multiphoton microscopy and confocal laser scanning microscopy. In parallel, the increased contrast of NP labeled particles (nCNF, nSF, nAF) allows for examination by imaging techniques based on X-ray radiation, such as SEM-EDX and μ-CT.

3.3. Multiphoton microscopy (MPM)

Multiphoton microscopy is a highly sensitive imaging technique, increasing the contrast by reducing the blurring of light. The local resolution is high, since exciting the fluorophores with two photons at the same time suppressed out-of-focus light. While the paper matrix was visualized by the second harmonic generation (grey), the signal of fluorophores (red) superimposed the paper matrix. All three stained types revealed significant differences in their morphology within the paper matrix (Fig. 3). The size of individual fibrils impeded their direct visualization but it can be seen that the fCNF aggregated and uniformly covered the macroscopic fibers (Bharimalla, Deshmukh, Patil, & Nadanathangam, 2017). The fSF tended to agglomerate on specific fiber-fiber junctions but a part also covered entire macroscopic fibers (Hobisch, Bossu et al., 2019; Mayr, Eckhart, & Bauer, 2017). fAF however showed an even distribution within the sheet.

Although MPM provided detailed insight on the distribution of cellulosic particles within a confined matrix, fluorescence microscopy is limited in resolution and measurements in z-direction. Therefore, the cross section of the paper sheets was investigated applying confocal laser scanning microscopy.

3.4. Confocal laser scanning microscopy

After embedding the paper sheets in resin and subsequent slicing, the materials were excitated at 405 and 532 nm, respectively. By recording

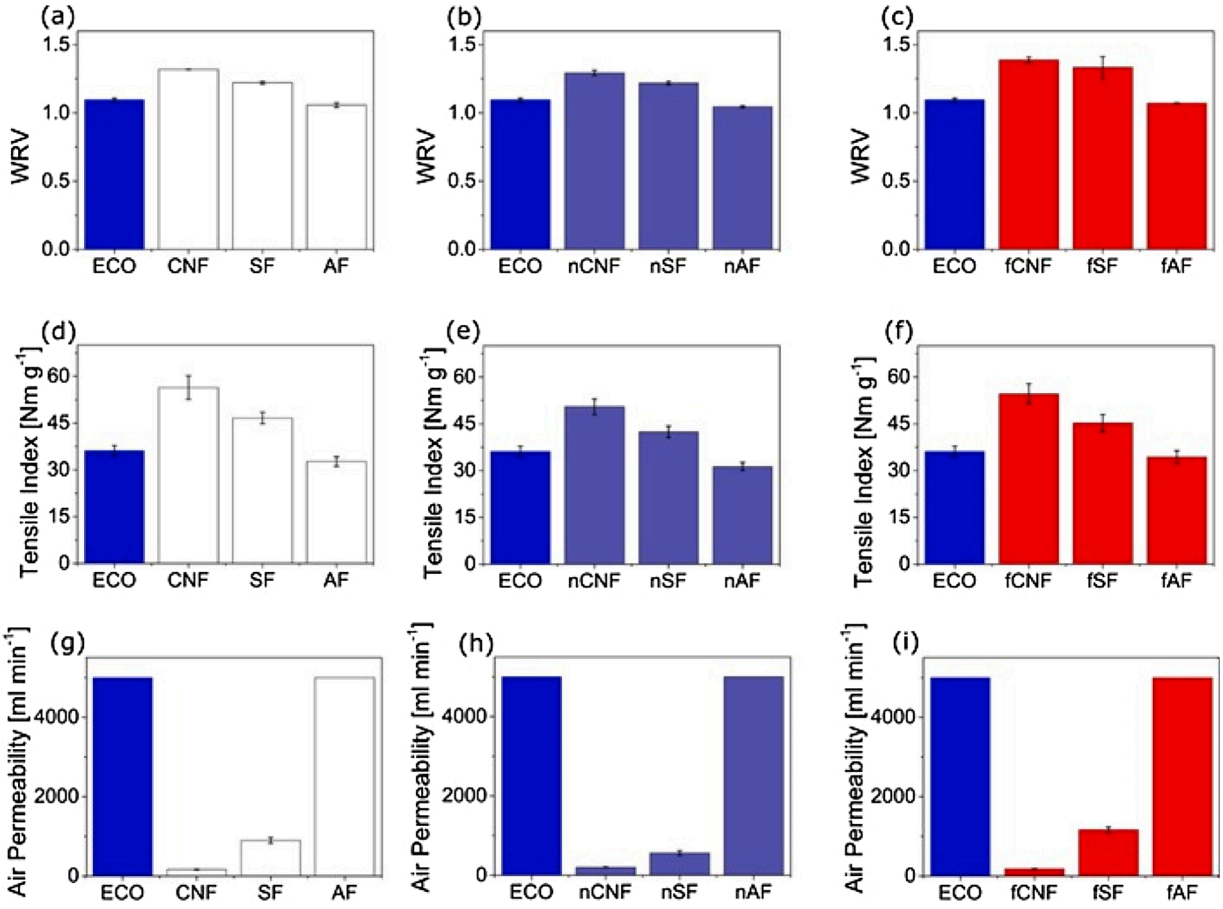

Fig. 2. Comparing physical and mechanical properties of papers containing untreated (a, d, g), nanoparticle labeled (b, e, h) and fluorescence labeled (c, f, i) cellulosic particles with the error bars showing the standard deviation of the samples. The investigation included water retention value of the pulp furnish (a-c), tensile index (d-f) and air permeability of the sheets (g-i).

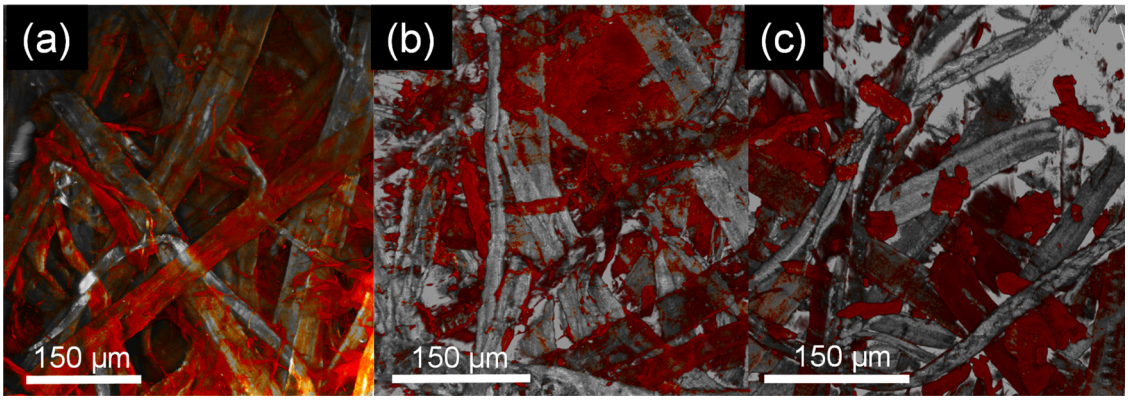

Fig. 3. Multiphoton microscopy images highlighting (a) fCNF (b) fSF and (c) fAF added to the sheet at 10 wt.%. Pulp fibers are depicted in grey while the fluorescent labeled samples are red.

the resulting emission, stained particles were visible (highlighted in red) within the fibrous network (Fig. 4). The fCNF gave a strong, homogeneous signal all over the cross section, indicating an even distribution in z-direction of the sheets. In contrast, the fSF and AF exhibited inhomogeneous intensity distributions, indicating a less homogeneous distribution inside the sheets along the z-direction. However, the resolution is not of sufficient quality for all the samples to obtain detailed information on spatial distribution of the materials, requiring further analysis using complementary techniques such as SEM and µCT.

3.5. Scanning electron microscopy with energy dispersive X-rays

SEM cross sectional analysis of the handsheets containing 10 % labeled particles, did not reveal any differences in morphology. Fig. S4 highlights the similarities in more detail. The same cross sections visualized by an EDX detector, however, yielded a distinct elemental distribution (Fig. 4). In some areas, we detected higher concentrations of Fe, Co, and O, which are the major components of the NPs used for the *in-situ* labeling process. The elemental distribution in those areas revealed a fibrous morphology, corresponding to the labeled fibrils inside the sheets. As sheets containing nCNF and nSF have a higher NP content (30 and 24 wt.%, respectively), the contrast was higher than for nAF, having a rather low NP content, impeding clear statements on their distribution inside the sheets. The nCNF seemed to be evenly distributed within the sheet, whereas nSF showed some tendency to agglomerate on the wire side (left).

3.6. X-ray microtomography

To visualize the labeled samples in a 3D manner in a large area, X-ray microtomography was employed. The results confirmed the results obtained by MPM and SEM-EDX but add a 3D component and allowed for slicing the paper sheet and to look inside the layers. However, data treatment is required prior to that and the use of a bandwidth color look up was required to reveal the details of the distribution of the nCNF, nSF and nAF inside the paper sheets. This procedure is widely accepted in analyzing such data and is based on reducing the thresholds for contrast resulting in different colors. Fig. S5 shows such a variation in threshold for the example of sheets with nSF. For all the samples the same threshold values as for Fig. S5a were chosen for the sake of comparability. In Fig. 5, slices are represented (Fig. 5a) and compared to the distribution of the labeled particles using the aforementioned data treatment, while retaining the sub-cellulose layer as base for a better understanding. Fig. S6 provides additional information for the handsheets containing nSF.

When looking at the different samples, the nCNF sample clearly

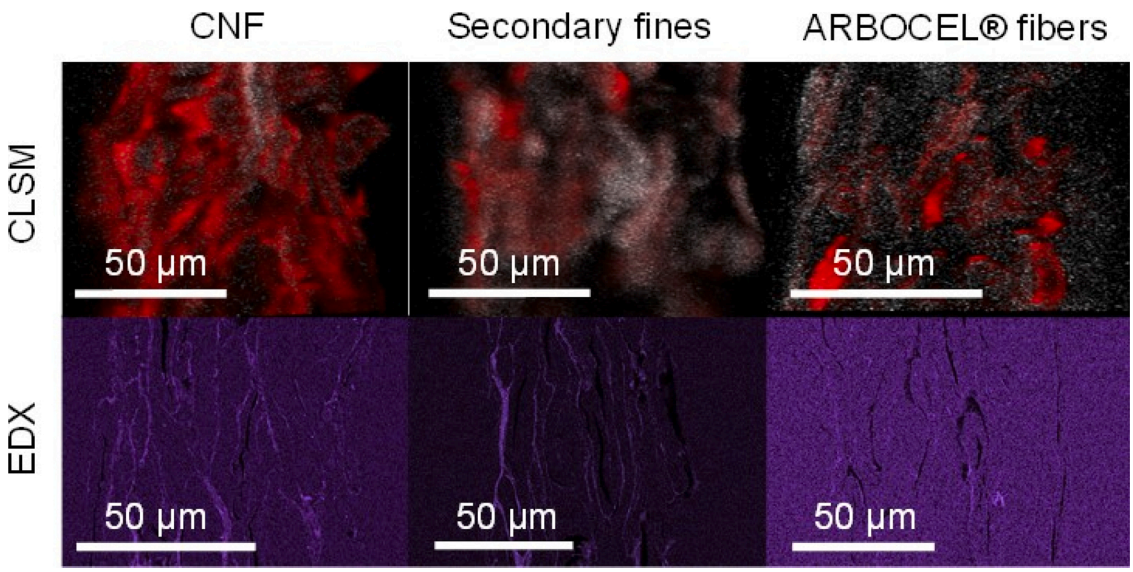

Fig. 4. Cross sections of paper sheets visualized by confocal laser scanning microscopy (top) and energy-dispersive X-ray of iron (bottom) showing huge differences between the different cellulosic particles, cellulose nanofibrils, secondary fines and ARBOCEL® fiber fragments (from left to right). The wire side in sheet formation correspond to left side in the SEM-EDX images.

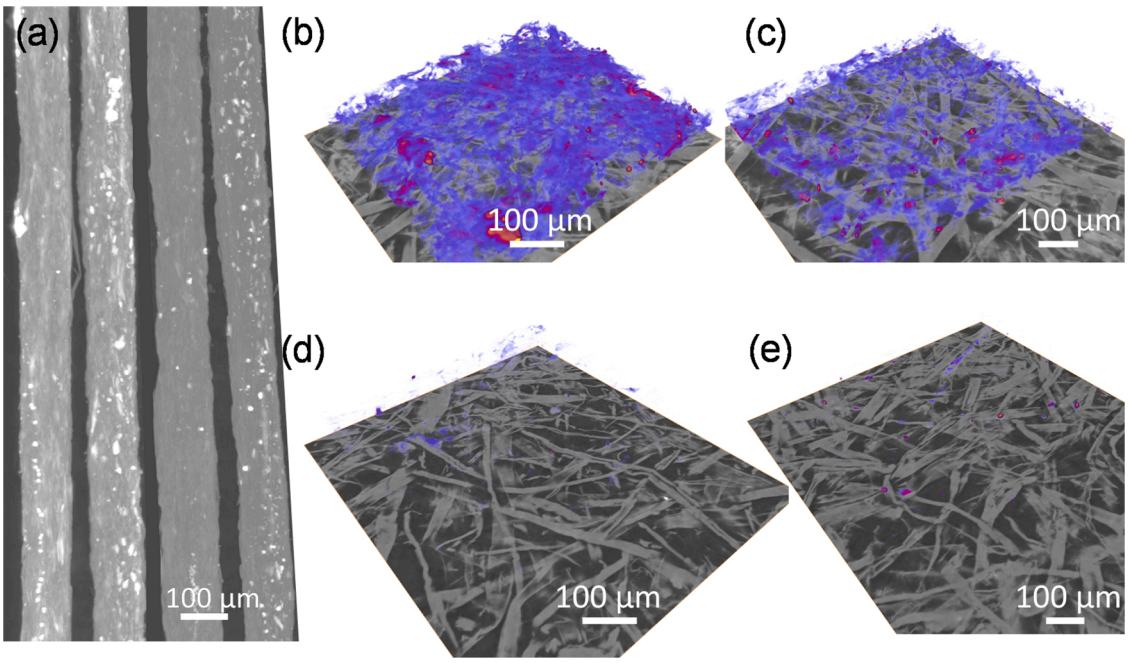

Fig. 5. X-ray microtomography data showing (a) the cross section of the paper stack (nCNF, nSF, nAF and CNF, from left to right) and the distribution of (b) cellulose nanofibrils, (c) secondary fines and (d) ARBOCEL® fiber fragments compared to a (e) blank containing 10 % untreated CNF.

shows that the CNF homogeneously covered the pulp fibers (Fig. 5b). Further, it seems that a 3D network is formed supporting a recently suggested idea that such a network is created when highly fibrillar material is present during paper making (Bossu et al., 2019; Boufi et al., 2016; Sehaqui, Allais, Zhou, & Berglund, 2011). Particularly, Berglund and coworkers connected the increase in tensile strength in paper sheets containing more than 10 % CNF to the coexistence of fiber networks at different length scales (micro, nano) (Sehaqui et al., 2011).

In contrast, nSF accumulate in the pores of the paper and seem to have higher concentrations in fiber-fiber junctions than nCNF (Fig. 5c). nAF labeled sheets exhibited a lack of contrast based on the low NP content (Fig. 5d) and hardly any differences to the blank were observed (Fig. 5e).

Furthermore, there are very intense spots which we originally deemed as artifacts (red colored small spheres). However, after thorough analysis, we identified these particles as $CaCO_3$ (see SEM-EDX in Fig. S7) which obviously stem from the process water of the pulp fibers and which could not be removed by the sheet forming process. Taking all data points from the µCT over the whole z-direction into account, nCNF and nSF slightly showed an uneven distribution in the thickness direction (Fig. 6). In contrast, for nAF such an orientation was not detected.

Nanko et al. (Nanko & Ohsawa, 1989) described the accumulation of fibrillar particles onto the fiber surface in the bonding region as the formation of a bonding layer, appearing with the presence of fines in the pulp. The interaction of external fibrils and secondary fines – both generated during pulp refining – enhanced the bonding properties and

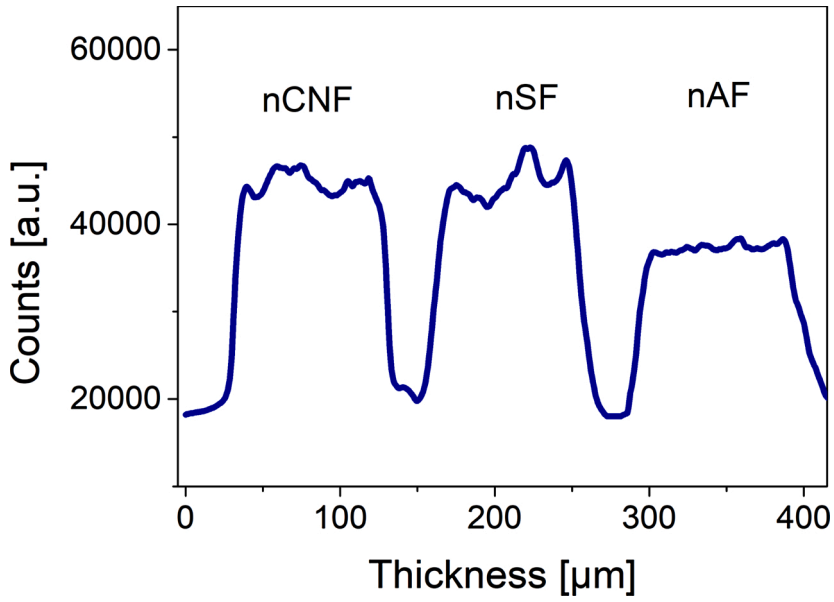

Fig. 6. Cross section in z-direction from the µ-CT data analysis from sheets containing nanoparticle labeled particles taking the entire signal of an area of 500 µm × 500 µm in width into account. The wire side is left for nCNF, and right for nSF and AF.

strengthened fiber-fiber joints in paper sheets. This in in agreement with our observation that the coarser SF are limited to the formation of new bridges, strengthening mainly already existing fiber-fiber bonds. CNF in turn also covers the pulp fibers, enabling the formation of new bonds between individual fibers. Thus, at higher addition levels CNF forms a secondary 3D network within the fiber network, thereby contributing to a densification of the paper sheet during sheet forming as predicted by Nanko et al. (Nanko & Ohsawa, 1989) and further explored by Favier et al. (Favier, Dendievel, Canova, Cavaille, & Gilormini, 1997). Water retention capacity is also much higher for CNF compared to SF and AF, leading to restricted mobility of the CNF during further dewatering and drying. Therefore, the formed 3D network of the CNF in the initial state of the sheet forming process was maintained. As a consequence, the distribution of the CNF inside the sheets is homogenous and any favored aggregation inside pores and fiber-fiber junctions, as observed for the SF, was not seen in any of our results. These results are again supported by the hypotheses of Nanko et al. who studied the influence of water contents of paper sheets as a function of drying time and fibrillation degree (Nanko & Ohsawa, 1989). Larger fragments such as AF are incapable of increasing fiber-fiber bonding, therefore the main parameters of the sheets did not change. This has also been reported by Sirviö et al. who studied the performance of paper sheets containing different types of fine materials (Sirviö & Nurminen, 2004). They reported that highly fibrillated fines had a positive impact on the tensile index (↑), and density (↑) while more flake like particles did not improve tensile index.

4. Conclusion

In summary, the distribution of nano- and micro-sized cellulosic particles in paper sheets was investigated by applying two independent labeling techniques and correlated to key properties of the sheets. As expected, the incorporation of particles with different degree of fibrillation impacted the paper sheet properties to different extents. We demonstrated that these properties were not altered significantly by the different labeling procedures. The major result was that CNF completely covers the macroscopic pulp fibers, while forming a dense 3D network inside the paper sheets. This network is probably the cause for the superior properties of sheets containing CNF (i.e. higher tensile index, higher density, lower air permeability). The SF in turn showed agglomeration in pores and fiber-fiber junctions, potentially revealing different reinforcement mechanisms (i.e. those reported by Nanko and Sirviö) compared to the CNF sheets. The AF samples were homogeneously distributed inside the paper sheets but they did not alter any of the sheet properties compared to the blank sample. This behavior can be explained by the lack of interactions with the pulp fibers and their inability to form a network due to their size. The combination of both methods revealed an unprecedented view on interactions between fibers and nano and micron sized cellulosic particles inside the sheets.

These results enable further investigations of the role of these smaller cellulosic particles in paper and board-based products and may be beneficial for the design of polymeric nanocomposites in the future. We are aware that additional features and complications may appear in scale-up experiments (e.g. alignment by shear/extrusion). These may impact the distribution of the nano/micron sized particles inside the matrix as well but these experiments were beyond the scope of this study as they require extensive equipment in semi-pilot scale.

A limitation of the current work is that is was not possible to determine the distribution of the different particles at very high resolution (low nm, as with SEM-EDX) throughout a whole sheet (as with μ-CT). Here, a further research direction could be to use an SEM which is equipped with a microtome to cut slices of the cross-section, to determine its elemental composition and to perform an image reconstruction afterwards. However, multiple challenges are to be addresses, ranging from choosing the right knife to cut the slices to problems in image reconstruction.

CRediT authorship contribution statement

Mathias A. Hobisch: Conceptualization, Methodology, Writing - original draft. **Simon Zabler:** Data curation, Visualization, Investigation. **Sylvia M. Bardet:** Data curation, Investigation. **Armin Zankel:** Data curation, Methodology, Investigation. **Tiina Nypelö:** Data curation, Writing - original draft, Writing - review & editing. **Rene Eckhart:** Writing - review & editing. **Wolfgang Bauer:** Conceptualization, Validation. **Stefan Spirk:** Supervision, Conceptualization, Methodology, Writing - review & editing.

Acknowledgments

The authors acknowledge the industrial partners Sappi Gratkorn, Zellstoff Pöls and Mondi Frantschach, the Austrian Research Promotion Agency (FFG), COMET, BMVIT, BMWFJ, the Province of Styria and Carinthia for their financial support of the K-project Flippr^2-Process Integration. Chonnipa Palasingh is acknowledged for assistance in carbohydrate composition determination.

Appendix A. Supplementary data

Supplementary material related to this article can be found, in the online version, at doi:https://doi.org/10.1016/j.carbpol.2020.117406.

References

Afra, E., Yousefi, H., Hadilam, M. M., & Nishino, T. (2013). Comparative effect of mechanical beating and nanofibrillation of cellulose on paper properties made from bagasse and softwood pulps. *Carbohydrate Polymers, 97*, 725–730.

Bardet, S. M., Carr, L., Soueid, M., Arnaud-Cormos, D., Leveque, P., & O'Connor, R. P. (2016). Multiphoton imaging reveals that nanosecond pulsed electric fields collapse tumor and normal vascular perfusion in human glioblastoma xenografts. *Scientific Reports, 6*, 34443.

Bharimalla, A. K., Deshmukh, S. P., Patil, P. G., & Nadanathangam, V. (2017). Micro/nano-fibrillated cellulose from cotton linters as strength additive in unbleached kraft paper: Experimental, semi-empirical, and mechanistic studies. *BioResources, 12*, 5682–5696.

Bossu, J., Eckhart, R., Czibula, C., Winter, A., Zankel, A., Gindl-Altmutter, W., et al. (2019). Fine cellulosic materials produced from chemical pulp: The combined effect of morphology and rate of addition on paper properties. *Nanomaterials, 9*, 321–338.

Boufi, S., Gonzalez, I., Delgado-Aguilar, M., Tarres, Q., Pelach, M. A., & Mutje, P. (2016). Nanofibrillated cellulose as an additive in papermaking process: A review. *Carbohydrate Polymers, 154*, 151–166.

Ding, Q., Zeng, J., Wang, B., Gao, W., Chen, K., Yuan, Z., et al. (2018). Effect of retention rate of fluorescent cellulose nanofibrils on paper properties and structure. *Carbohydrate Polymers, 186*, 73–81.

Favier, V., Dendievel, R., Canova, G., Cavaille, J. Y., & Gilormini, P. (1997). Simulation and modeling of three-dimensional percolating structures: Case of a latex matrix reinforced by a network of cellulose fibers. *Acta Materialia, 45*, 1557–1565.

Fischer, W. J., Mayr, M., Spirk, S., Reishofer, D., Jagiello, L. A., Schmiedt, R., et al. (2017). Pulp fines-characterization, sheet formation, and comparison to microfibrillated cellulose. *Polymers, 9*, 366.

Fischer, W. J., Zankel, A., Ganser, C., Schmied, F. J., Schroettner, H., Hirn, U., et al. (2014). Imaging of the formerly bonded area of individual fibre to fibre joints with SEM and AFM. *Cellulose, 21*, 251–260.

Giner Tovar, R., Fischer, W. J., Eckhart, R., & Bauer, W. (2015). White water recirculation method as a means to evaluate the influence of fines on the properties of handsheets. *BioResources, 10*, 7242–7251.

Hobisch, M. A., Bossu, J., Mandlez, D., Bardet, S. M., Spirk, S., Eckhart, R., et al. (2019). Localization of cellulosic fines in paper via fluorescent labeling. *Cellulose, 26*, 6933–6942.

Hobisch, M. A., Muller, D., Fischer, W. J., Zankel, A., Eckhart, R., Bauer, W., et al. (2019). Cobalt ferrite nanoparticles for three-dimensional visualization of micro- and nanostructured cellulose in paper. *ACS Applied Nano Materials, 2*, 3864–3869.

Huang, L., He, L., Gao, W., Zeng, J., Wang, B., Xu, J., et al. (2020). Distribution analysis of cellulose nanofibrils in paper handsheets: Dye-labeled method. *Carbohydrate Polymers, 239*, Article 116226.

Hyll, K., Farahani, F., & Mattsson, L. (2016). Optical methods for fines and filler size characterization. *Innventia Report, 71*, 52.

Kang, T., & Paulapuro, H. (2006). Effect of external fibrillation on paper strength. *Pulp & Paper Canada, 107*, 51–54.

Krogerus, B., Fagerholm, K., & Tiikkaja, E. (2002). Fines from different pulps compared by image analysis. *NPPRJ, 17*, 440–444.

Mayr, M., Eckhart, R., & Bauer, W. (2017). Improved microscopy method for morphological characterisation of pulp fines. *NPPRJ, 32*, 244–252.

Nanko, H., & Ohsawa, J. (1989). Mechanisms of fibre bond formation. In C. F. Baker, & V. W. Punton (Eds.), *Fundamentals of Papermaking Trans. IXth Fund. Res. Symp.*.

Nechyporchuk, O., Belgacem, M. N., & Bras, J. (2016). Production of cellulose nanofibrils: A review of recent advances. *Industrial Crops and Products, 93*, 2–25.
Odabas, N., Henniges, U., Potthast, A., & Rosenau, T. (2016). Cellulosic fines: Properties and effects. *Progress in Materials Science, 83*, 574–594.
Olsson, R. T., Azizi Samir, M. A., Salazar-Alvarez, G., Belova, L., Ström, V., Berglund, L. A., … Gedde, U. W. (2010). Making flexible magnetic aerogels and stiff magnetic nanopaper using cellulose nanofibrils as templates. *Nature Nanotechnology, 5*, 584–588.
Purington, E., Bousfield, D., & Gramlich, W. M. (2019). Fluorescent dye adsorption in aqueous suspension to produce tagged cellulose nanofibers for visualization on paper. *Cellulose, 26*, 5117–5131.
Reid, M. S., Karlsson, M., & Abitbol, T. (2020). Fluorescently labeled cellulose nanofibrils for detection and loss analysis. *Carbohydrate Polymers, 250*, Article 116943.
Salari, M., Bitounis, D., Bhattacharya, K., Pyrgiotakis, G., Zhang, Z., Purington, E., et al. (2019). Development & characterization of fluorescently tagged nanocellulose for nanotoxicological studies. *Environmental Science Nano, 6*, 1516–1526.
Sehaqui, H., Allais, M., Zhou, Q., & Berglund, L. A. (2011). Wood cellulose biocomposites with fibrous structures at micro- and nanoscale. *Composites Science and Technology, 71*, 382–387.
Sirviö, J., & Nurminen, I. (2004). Systematic changes in paper properties caused by fines. *Pulp & Paper Canada, 105*, 39–42.
TAPPI. (1994). *Test method t 261 cm-94. Fines fraction of paper stock by wet screening*.
Theander, O., & Westerlund, E. A. (1986). Studies on dietary fiber. 3. Improved procedures for analysis of dietary fiber. *Journal of Agricultural and Food Chemistry, 34*, 330–336.
Yousefi, H., Azad, S., Mashkour, M., & Khazaeian, A. (2018). Cellulose nanofiber board. *Carbohydrate Polymers, 187*, 133–139.
Zabler, S., Ullherr, M., Fella, C., Schielein, R., Focke, O., Zeller-Plumhoff, B., et al. (2019). Comparing image quality in phase contrast subμ x-ray tomography–A round-robin study. *arXiv preprint arXiv:1905.02651*.